Effects of scaling laws on the combustion and NO_x characteristics of hydrogen burners

Christoph Meraner[a,*], Tian Li[a], Mario Ditaranto[b], Terese Løvås[a]

[a] *Department of Energy and Process Engineering, Faculty of Engineering, NTNU – Norwegian University of Science and Technology, Trondheim, Norway*
[b] *SINTEF Energy Research, Trondheim, Norway*

Abstract

The effect of constant velocity and constant residence time scaling on the local nitric oxide (NO_x) emissions and flame characteristics of complex partial premixed hydrogen burners were investigated numerically and theoretically. A previously developed and validated computational fluid dynamic (CFD) model was employed to conduct in total 11 simulations at various burner scales ranging from a base case of 10 kW to an up-scaled burner design at 500 kW. The flame characteristics were investigated by means of a novel CFD based regime diagram and compared to Damköhler and Karlovitz numbers obtained from scaling theory. The flame is at laboratory scale mainly characterized by the thin reaction zone regime. Employing constant velocity scaling was predicted to overall decrease the Karlovitz number, which causes the combustion to appear partially in the corrugated flamelet regime and at scales exceeding 250 kW also in the wrinkled flamelet regime. Constant residence time scaling on the other hand leads overall to a combustion with constant Damköhler numbers. However, for a constant Karlovitz number close to unity was observed for a significant part of the flame-sheet, which leads in this flame regions to a variable Damköhler number. Both investigated scaling principles lead to an increase of the overall NO_x emissions, with constant velocity scaling resulting in the highest emissions. This is mainly attributed to the larger volumes and longer

*Corresponding author
Email address: christoph.meraner@ntnu.no (Christoph Meraner)

This is the accepted version of an article published in Combustion and Flame
http://dx.doi.org/10.1016/j.combustflame.2020.01.010

residence times of the flame and immediate post flame region compared to constant residence time scaling. The total NO_x formation in the inner recirculation zone, on the other hand, is lower for constant velocity scaling and is found to be dominated by the local oxygen atom (O) and hydroxyl (OH) concentration. Constant velocity scaling causes a breakup of the inner recirculation zone at the 500 kW scale, which leads to a fundamentally different flow field and causes the flame to impinge onto the combustion chamber wall, whereas constant residence time scaling maintains the inner recirculation zone at all investigated scales. The breakup of the recirculation zone is attributed to the different effect of the scaling principles on the velocity to length scale ratio and momentum of the annular jet flow.

Keywords: scaling, NO_x emission, hydrogen, partially premixed burner, combustion regime diagram

---

Nomenclature

Symbols

A, A', B_1, B_2, C, C' markers

D diameter (m)

K proportionality constant (-)

k turbulent kinetic energy (m^2 s^{-2})

L_{IRZ} inner recirculation zone length(m)

l length scale (m)

l' turbulent length scale (m)

This is the accepted version of an article published in Combustion and Flame
http://dx.doi.org/10.1016/j.combustflame.2020.01.010

Q thermal input (W)

S_L laminar flame speed (m s^{-1})

U velocity (m s^{-1})

u cartesian velocity component (m s^{-1})

u' turbulent velocity scale (m s^{-1})

Y mass fraction (-)

y spacial coordinate (m)

Greek

β scaling factor (-)

δ_L laminar flame thickness (m)

ϵ dissipation rate (m^2 s^3)

η_k Kolmogorov length scale (m)

ν kinematic viscosity (m^2 s^{-1})

ρ density (kg m^{-3})

τ_c chemical time scale (s)

τ_k Kolmogorov time scale (s)

τ_T turbulent time scale (s)

Dimensionless groups

This is the accepted version of an article published in Combustion and Flame
http://dx.doi.org/10.1016/j.combustflame.2020.01.010

Da Damköhler number

Ka Karlovitz number

Re Reynolds number

Subscript

0 burner characteristic

ax axial direction

rt constant residence time

v constant velocity

Superscript

* scaled

eq chemical equilibrium

Abbreviations

CFD computational fluid dynamic

EDC eddy dissipation concept

FL flame

IPF immediate post flame

IRZ inner recirculation zone

MILD moderate or intense low-oxygen dilution

This is the accepted version of an article published in Combustion and Flame
http://dx.doi.org/10.1016/j.combustflame.2020.01.010

NO_x nitric oxide

ORZ outer recirculation zone

PDF probability density function

PF post flame

PPBB partially premixed bluff body

RANS Reynolds averaged Navier-Stokes

WJ wall jet

1. Introduction

Increasingly stringent regulations on emissions from stationary power and heat production has motivated the development of various low emission technologies, including carbon capture and storage units, flexi-fuel units enabling the use of non-carbon containing fuels such as hydrogen and recently ammonia [1], and various low and ultra low NO_x burners over the last decades. For the latter, dry low emission (DLE) combustion has traditionally been the most common used technology to reduce NO_x emissions [2]. DLE combustion is dependent on highly controlled mixing of air and fuel to achieve lean premixed combustion, thereby reducing the flame temperature and hence reducing NO_x formation. Due to the reduced temperatures, special considerations have to be made, to ensure an environment that at the same time does not promote unacceptable levels of unburnt hydrocarbons and carbon monoxide (CO), as well as combustion instabilities. When considering high hydrogen content fuels, other issues come into play. Higher burning velocities and temperatures need to be carefully controlled by design optimization to avoid flashbacks. As a result, burners with complex flow regimes have been proposed. This involves for example swirl burners [3], flame-sheet burners [4], micro-mixing burners [5] and recently partially premixed bluff body burners [6, 7]. Common

This is the accepted version of an article published in Combustion and Flame
http://dx.doi.org/10.1016/j.combustflame.2020.01.010

for these burners are highly optimized flows and complex designs in order to obtain optimum low emission, yet efficient operation.

The high cost associated with the development process of such complex burners motivates experiments and numerical simulations at laboratory scale. This requires scaling of the burner geometry by employing scaling laws that preserve the burner characteristics at different burner sizes. However, the large number of scaling parameters found through similarity theory, many of them mutually incompatible, make a complete scaling practically impossible. Scaling problems are therefore treated by the use of partial scaling, which has been reviewed in detail by Spalding [8] and Beér [9]. Thus a variety of different scaling laws can be found in literature, the majority of which have been developed for "simple" axisymmetric, turbulent, jet flames, which provide a well-defined flow field [10]. However, for industrial burners typically only two scaling laws are considered, namely constant velocity (i.e., the characteristic burner velocity, U_0, is kept constant while increasing the burner dimensions) and constant residence time scaling (i.e., the ratio between the characteristic burner length scale and velocity scale, D_0/U_0, is kept constant while increasing the burner dimensions) [11]. Both approaches are based on the basic global equation for the thermal input, Q:

$$Q = K\rho_0 U_0 D_0^2, \tag{1}$$

where K is a proportionality constant and ρ_0 the inlet fluid density. They, furthermore, demand geometrical similarity, hence all dimensions can be derived from the scaled characteristic burner length scale, D_0^*, and assume that the Reynolds and Froude number are sufficiently large, so that the burner flow is turbulent and momentum controlled (i.e., buoyancy effects are neglected) at all relevant scales. By keeping the characteristic velocity, U_0, constant and considering equation (1) the scaled burner diameter for constant velocity scaling can be derived from the following relation:

$$\frac{D_{0,v}^*}{D_0} \propto \left(\frac{Q_v^*}{Q}\right)^{1/2}. \tag{2}$$

The objective of constant residence time scaling is to preserve the convective timescale, which represents the residence time for simple flames, by maintaining the ratio D_0/U_0 constant and hence

This is the accepted version of an article published in Combustion and Flame
http://dx.doi.org/10.1016/j.combustflame.2020.01.010

preserving in theory the macro-mixing characteristics of a burner [11, 12]. By obeying this requirement together with equation (1), constant residence time scaling can be described as:

$$\frac{D^*_{0,rt}}{D_0} \propto \left(\frac{Q^*_{rt}}{Q}\right)^{1/3}. \tag{3}$$

The effect of these two scaling laws on the macro- and micro-mixing is further elaborated in appendix A.

The first studies concerning the scalability of NO_x emissions aimed to develop scaling laws based on equilibrium conditions for temperature and oxygen atom (O) concentration such as the study by Lavoie and Schlander [13] and the asymptotic analysis by Peters [14]. However, flame stretch can lead to a significant departure from equilibrium conditions, as has been shown by Drake and Blint [15], as well as by Barlow and Carter [16, 17]. Various scaling models have, therefore, been proposed that consider non-equilibrium conditions, which led to the finding that NO_x emissions can be characterized by a negative one-half power dependency on the flame Damköhler number (i.e., the ratio of the characteristic time scale for macro-mixing to the characteristic chemical time scale) [18–21]. Szego et al. [22] suggested that, under certain conditions, all parameters affecting global NO_x emissions can be characterized by a global residence time and furnace temperature as proposed by Turns et al. [23, 24], following the hypothesis that a majority of the NO_x emissions are formed in large and nearly homogeneous eddies [25]. The scaling law proposed by Røkke et al. [26] is one of few studies regarding NO_x emissions from partially premixed flames and was re-evaluated by Santos and Costa [27] for turbulent diffusion flames. Weber [12] concluded the effect of flue gas entrainment, from internal and external flue gas recirculation, and the radiation heat loss in the post flame need to be included in order to make the correlation by Røkke et al. [26] applicable to industrial burners.

An important work regarding constant velocity scaling was conducted in the Scaling-400 project [28] which led to an extensive data set for the NO_x emission performance of swirl burners in the range of 30 kW to 12 MW thermal input. The project was later extended to constant residence time scaling by means of numerical simulations [29]. Several studies of pulverized coal burners [30–32] as well

This is the accepted version of an article published in Combustion and Flame
http://dx.doi.org/10.1016/j.combustflame.2020.01.010

as gas burners [29, 33, 34] compared constant velocity scaling and constant residence time scaling with each other. It is worth noticing that there is no consensus on one of these two scaling laws being superior over the the other. Smart and Van Kamp [31] found that neither constant velocity nor constant residence time scaling were able to preserve flame structures and thermochemical fields adequately when scaling a pulverised coal burner. Furthermore, their study indicated the existence of a minimum scale which is still representative for a full-scale burner and showed that both scaling laws lead to a weakening of the inner recirculation zone.

The work by Weber and Mancini [35] provides the most recent overview on scaling of large scale industrial flames. They emphasise that: "the scaling issue disappeared from the research agenda" for almost two decades, which left many questions unanswered. This is especially true for partially premixed flames, which are addressed in the present paper. Furthermore, only a limited number of studies is found in the literature that investigate local scaling effects in different burner regions and treat these regions individually [36, 37]. It is however expected that scaling of modern burners, following the constant velocity or the constant residence time approach, will exhibit local scaling effects due to the complex nature of the burner designs, which is not adequately represented by a single length and velocity scale [36]. The objective of the present work is to develop a deeper understanding of the scaling effects on the flame structure and NO_x formation in different regions of complex modern burners. The study case presented is a partially premixed bluff body (PPBB) burner which consists of inner and outer recirculation zones, stagnation points, staged fuel injection and varying degree of partial premixing. Hence, the burner shares many of the characteristics found in complex industrial burners, but still allows the understanding of general scaling effects. The impact of different scaling laws on the combustion regimes and NO_x emissions performance of this complex burner are investigated with hydrogen as fuel. Using hydrogen as fuel has the double advantage of focussing on a single NO_x formation route and to relieve the computational effort. Besides, hydrogen is foreseen to be a dominant fuel in the low carbon society needed to achieve the global climate change targets. The scope comprises furthermore the identification of potentially critical thermal

This is the accepted version of an article published in Combustion and Flame
http://dx.doi.org/10.1016/j.combustflame.2020.01.010

loads that may limit the scalability of the burner, which have for example been found for the scaling of pulverized coal [30] and natural gas burners [29]. The present work addresses the lack of research regarding scaling of complex burners and aims to fill the knowledge-gap by investigating scaling effects through the analysis of local combustion regimes and NO_x formation in different regions of the flames.

The scaling effects are investigated based on a set of 11 computational fluid dynamic (CFD) simulations at different scales up to a thermal load of 500 kW. The paper presents first the impact of the scaling approaches on the combustion characteristics in general. This is done by means of combustion regime diagrams combined with hexagon binning and the analysis of the progress variable source term distribution. In addition to the CFD based results theoretical considerations are presented. Finally the work focuses on NO_x emissions and scrutinizes the contribution of different flow regions to the NO_x formation.

2. Methodology

2.1. Burner design

The present work is based on the scaling of the PPBB burner, developed by Spangelo et al. [38]. This burner is intended for the use in boilers and furnaces that typically operate at pressures close to atmospheric and with approximately 3% excess air. An illustration of the burner can be seen in figure 1. The PPBB burner employs a frustum shaped conical bluff body to stabilise the flame and allows for the dilution of the fuel-air mixture by internally recirculated flue gas. Fuel is partially premixed via jets in an accelerating cross-flow. The degree of premixing can be adjusted via eight primary and four secondary fuel ports. The primary fuel ports are located upstream of the burner throat in a converging burner section formed by the burner housing. The secondary fuel ports are located downstream of the burner throat. Primary and secondary fuel ports are, in angular direction, offset to each other such that the secondary fuel ports are located in between every other pair of

This is the accepted version of an article published in Combustion and Flame
http://dx.doi.org/10.1016/j.combustflame.2020.01.010

primary fuel ports. The burner was in recent years investigated experimentally by Dutka et al. [6, 39–41] and numerically by Meraner et al. [42, 43] for the combustion of hydrogen and hydrogen enriched fuels. Further details on the burners operational characteristics can be found therein.

2.2. Numerical methods

The numerical model that was employed for the simulations of the PPBB burner has been developed and validated against experimental data in previous work [42, 43]. A detailed description as well as a discussion on modelling uncertainties can be found in the corresponding publications. Hence, only a short summary is given here. The model was developed with the simulation of larger scales in mind. Reducing computational costs have therefore been given a high priority, which resulted in a model based on steady state, incompressible, Reynolds averaged (RANS) governing equations. Another important aspect of choosing a relatively inexpensive numerical model is the possibility to cover a wider range of burner scales. Steady state RANS simulations are order of magnitudes less computationally expensive than for example large eddy simulations. This is not only due to the lower special resolution needed for RANS simulations, but also due to the possibility to apply the steady state assumption and to utilize the periodicity of the burner (i.e., reduce the simulation to one quarter of the domain). The computational costs are further reduced by invoking non-equilibrium wall functions and by employing a post processing approach for the NO_x calculation, i.e. the NO_x calculation is decoupled from the combustion kinetics and based on a "frozen" combustion simulation. The eddy-dissipation concept (EDC) [44, 45] in combination with a detailed combustion mechanism for the hydrogen oxidation by Li et al. [46], containing 9 species and 19 reversible reactions, was used to model the turbulent combustion process. A crucial property of the EDC is that its applicability is not restricted to certain combustion regimes. RANS-EDC based models have already been successfully applied to comparable burner configurations [47, 48]. Based on these studies, a tendency to over-predict temperatures can be expected. The discrete ordinates radiation model was employed to account for thermal radiation. The diffusive mass flux was calculated based on the dilute approx-

This is the accepted version of an article published in Combustion and Flame
http://dx.doi.org/10.1016/j.combustflame.2020.01.010

imation (i.e., Fick's law) for turbulent flows. A grid independency study, comprising meshes ranging from 3.5 M to 14.4 M cells, was conducted for the burner at 100 kW and 500 kW scales assuming that it is valid for the intermediate scales with lower Reynolds numbers as well.

The only deviation from the original model setup presented by Meraner et al. [43] are the thermal boundary conditions for the lateral surfaces of the bluff body. These were originally modelled adiabatic. The present study has, however, shown that this unrealistic assumption leads, at certain scales, to a flame flashback within the boundary layer. The lateral bluff body walls have therefore been modelled with a constant temperature of 293 K, corresponding the air inlet temperature. A sensitivity analysis has shown that this change does not affect the global NO_x emissions.

3. Results and discussion

This section scrutinizes initially the impact of the two applied scaling laws on the burner characteristics, when the burner is scaled from laboratory scale to 50 kW and 250 kW respectively. This is followed by an analysis of NO_x emissions at different scales and parameters that are relevant for the NO_x formation. Finally the simulation of the PPBB burner with a thermal input of 500 kW, scaled using the constant velocity scaling approach, is analysed since it reveals a special case of a fundamentally different flow structure compared to all other cases.

3.1. Combustion regime and flame characteristics

Regime diagrams have historically been developed based on the interaction of homogeneous and isotropic frozen (i.e., unaffected by heat release) turbulence with a premixed flame. In order to utilize them for the partially premixed burners, special considerations need to be made. Meraner et al.[43] proposes to extract data from CFD simulations on a predefined iso-surface that is close enough to the flame, so that the mixture composition is representative for the combustion, but at a distance where the turbulence is not yet heavily affected by the heat release. This is achieved by defining an iso-surface of 5% of the maximum heat release rate, which is then clipped using a normalized

This is the accepted version of an article published in Combustion and Flame
http://dx.doi.org/10.1016/j.combustflame.2020.01.010

progress variable (i.e., $(Y_{HO_2} + Y_{H_2O})/(Y_{HO_2} + Y_{H_2O})^{eq}$) of 0.5 as an upper limit to ensure that the data is collected on the reactants side of the flame. The data obtained on this surface is then used to categorize the flame by means of regime diagrams. Utilizing such scatter data provides a more refined insight into the burner characteristics compared to the traditional approach of describing the entire burner by a single point in the regime diagram, especially for combustion in burners which likely occurs in a multi regime mode. Representing the burner by a scatter plot furthermore allows the visualization of dependencies between local conditions, such as the equivalence ratio, and the combustion regimes. However, the overlapping of data points in densely populated scatter plots can make it difficult to identify the most representative regimes. Alternatively, hexagon binning [49], a form of bivariate histogram, can be utilized to assign a more accurate weight to different combustion regimes. This approach is employed in Figure 2 which shows the modified turbulent combustion diagram based on Peters [50] for five different CFD simulations. Here, each visible bin contains at least one data point and the colour assigned to it indicates the volume fraction that is represented by the bin. The volume calculations are based on the volume of the cells that are intersected by the predefined iso-surface. The global representation of the burner is marked by a single circular marker. The turbulent length scale, l', and the turbulent velocity scale, u', for this point are based on the area weighted average conditions in the burner throat. The laminar flame speed, S_L, and laminar flame thickness, δ_L, were calculated in the open-source software Cantera [51] based on the global equivalence ratio of the burner. In addition the effect of scaling on the flame characteristics in a global context, based on scaling theory (see appendix A) is outlined by a red and orange line respectively.

At laboratory scale most of the flame falls into the thin reaction zone (i.e., $1 < Ka < 100$) and the corrugated flamelet (i.e., $Ka < 1$ and $u'/S_L > 1$) regimes, with the Karlovitz number, Ka, defined as the ratio between the characteristic chemical time scale to the Kolmogorov (i.e., micro-mixing) time scale. From previous work [43] we know that the two distinct regions seen at laboratory scale in figure 2 between $Da = 1$ and $Ka = 1$, with a volume fraction exceeding 2%, are attributed to the

This is the accepted version of an article published in Combustion and Flame
http://dx.doi.org/10.1016/j.combustflame.2020.01.010

primary and secondary fuel streams at a equivalence ratios close to stoichiometry. The primary fuel stream is characterized by lower length scale ratios compared to the secondary fuel stream. Fuel lean flame regions fall mainly within $Ka <= 100$ and $Da <= 1$ where the Karlovitz number increases with decreasing equivalence ratio due to the decreasing flame speed.

For constant velocity scaling, both the global representation of the burner as well as the peak values of the hexbin plot follow the line for the theoretical scaling. At larger scales, parts of the flame cross into the wrinkled flame regime (i.e., $u'/S_L < 1$). It can furthermore be seen that the regions assigned to the primary and secondary fuel ports are less distinct from each other with increasing thermal input and collapse to the same location at the 250 kW scale. The same is true for constant residence time scaling, where they collapse as well at 250 kW. However, the overall trend for constant residence time scaling is different. The global representation of the burner and the overall distribution shown in the hexbin plot follow the theoretical scaling with a constant Damköhler number relatively close. The peak values in the hexbin plot, however, appear to lie on an iso-line for the Karlovitz number close to unity. This is important for smaller burner scales where temperature and NO_x formation are more affected by micro-mixing compared to large scales where macro-mixing and hence the Damköhler dependency dominates [35].

Figure 3 shows the scatter data of the 250 kW configuration coloured by the local equivalence ratio. The data points for the scatter plots are sorted by their distance to the stoichiometric mixture fraction. Hence, data points closer to the stoichiometric mixture overlay points that are further away from stoichiometry, independent on which side (i.e., fuel lean or rich) they are located. For both scaling approaches, a "flare" of lean data points can be seen that is leading towards larger Karlovitz numbers, due to the reduced flame speed at lean mixture fractions. Constant residence time scaling preserves the two distinct bands with a stoichiometric equivalence ratio, which have been identified by Meraner et al. [43] for the base case. Constant velocity scaling, on the other hand, shows a wider scatter of the stoichiometric mixture in the regime diagram and less distinct bands. Generally a stronger separation of lean, rich and stoichiometric mixtures within the regime diagram

This is the accepted version of an article published in Combustion and Flame
http://dx.doi.org/10.1016/j.combustflame.2020.01.010

can be seen for constant residence time scaling, where rich equivalence ratios show the largest and stoichiometric equivalence ratio the least variation. Note, the data points that follow a constant Karlovitz number show little variation and cannot be attributed to a certain equivalence ratio. An important parameter for the flame speed and thickness is the dilution by entrained combustion products, which cannot be identified based on the equivalence ratio only. However, mixtures close to the stoichiometric equivalence ratio respectively are expected to show less variation in the amount of entrained products, while mixture that are further away are expected to show more variation, which translates in a wider spread in flame speed and thickness.

Figure 2 and figure 3 are per definition restricted to the flame leading edge. Figure 4, on the other hand, provides an overview on the combustion process in the whole domain by integrating the progress variable source term (i.e., $R_{HO_2} + R_{H_2O}$) along the axial and radial coordinates. This allows the visualization of its probability density distribution in a two dimensional space, defined by the angular coordinate and the local equivalence ratio. Figure 4 shows results from the same simulations as figure 2. The fuel port location of $+/-22.5°$ for the primary and $0°$ for the secondary fuel is for all cases recognizable by peaks in the equivalence ratio marked as B_1 and B_2. The difference between the peak equivalence ratios (i.e. B_2 - B_1) in the two different fuel streams increases when constant velocity scaling is employed and is more than twice as big for the 250 kW case compared to the base case. Furthermore, both values, B_1 and $B_{2,}$ are at richer equivalence ratios. This trend is opposite for constant residence time scaling where both peaks are at lower equivalence ratios and slightly closer in value to each other, when comparing the 250 kW and 10 kW simulations.

Another difference between constant velocity and constant residence time scaling can, however, be seen in between primary and secondary fuel ports marked as point A and C respectively. Constant velocity scaling leads here (see A), with increasing thermal input, to an increase of the local progress variable source term. This can also be seen in the form of a second peak in the marginal plot marked as A', which does not appear when constant residence time scaling is employed. The probability density distribution of the progress variable source term reaches for all cases its maximum around

This is the accepted version of an article published in Combustion and Flame
http://dx.doi.org/10.1016/j.combustflame.2020.01.010

stoichiometry. However, this peak is more significant for larger thermal input and constant residence time scaling, which can be seen in location D. This indicates, in combination with the "discontinuity" point C, that the fuel streams on a macro scale are less premixed compared to the constant velocity scaling. Indeed, figure 5, which shows the stoichiometric iso-surface for the five different CFD simulations, reveals that each of the fuel stream is recognizable as a single "jet" at 250 kW when constant residence time scaling is applied. All other simulations show a continuous, though wrinkled, iso-surface and hence a fuel rich inner recirculation zone. Note that all subfigures are scaled to the same bluff body diameter. It can also be seen that the iso-surface is characterized by four tips that move closer together for constant velocity scaling and finally collapse to a single tip at 250 kW, while they get further separated when constant residence time scaling is applied.

This is the accepted version of an article published in Combustion and Flame
http://dx.doi.org/10.1016/j.combustflame.2020.01.010

3.2. NO_x formation

The stoichiometric iso-surface in figure 5 is coloured by the volumetric NO_x formation rate. The peak rate is in all cases reached in between primary and secondary fuel ports in the concave region formed by the iso-surface. This is in general the location where a stoichiometric mixture of fuel and combustion air meets hot products that are recirculated in the inner recirculation zone. At laboratory scale of 10 kW the peak values appear as a single region spanning from the primary to the secondary fuel stream. Scaling the burner up by means of constant velocity scaling leads to the formation of two separate elongated regions with elevated NO_x formation rates that merge again after a certain distance downstream of the bluff body trailing edge. The local peak formation rate on the stoichiometric iso-surface for constant residence time scaling is, however, generally lower compared to the constant velocity scaling approach. The two scaling approaches lead to a significant different appearance of the iso-surface at 250 kW. Even though clear differences can be seen in figure 5 it is not possible to conclude on the overall NO_x performance based on a local volumetric source term as the volumes for the different scaling approaches are significantly different. Figure 6 shows the global NO_x emissions at different scales for constant velocity and constant residence time scaling. Both methodologies lead to increasing NO_x emissions at increasing scales. However, constant velocity scaling reaches higher NO_x levels. None of the approaches reaches a plateau within the investigated range. Note, that the largest reported simulation for constant velocity scaling in this section is 450 kW; the 500 kW case is a special case and will be discussed in section 3.3.

The fluid domain was subdivided into six sub domains during post processing, similar to the approach presented by Hsieh et al. [36], in order to identify regions that contribute to the trend seen in figure 6. The regions are the wall jet (WJ), flame (FL), inner recirculation zone (IRZ), outer recirculation zone (ORZ), immediate post flame (IPF) and post flame (PF) as illustrated in figure 7.

Figure 8 presents the total NO_x formation rate based on the described domain subdivision. For clarity, only the three main contributing regions, immediate post flame, flame and inner recirculation zone are shown. The formation rate for all other regions is in general more than one order of

This is the accepted version of an article published in Combustion and Flame
http://dx.doi.org/10.1016/j.combustflame.2020.01.010

magnitude smaller than the formation rate in the inner recirculation zone, confirming the findings by Hsieh et al. [36]. The constant velocity approach leads, with increasing scales, to a more rapid increase of the formation rate in the immediate post flame and flame region compared to constant residence time scaling. The inner recirculation zone on the other hand shows an opposite trend. The rate increases here for constant residence time scaling, while it stays relatively constant for constant velocity scaling.

The inner recirculation zone and the flame region are dominating in terms of a mean volumetric rate as shown in figure 9. Constant residence time scaling leads in all three regions to larger mean volumetric NO_x formation rate than constant velocity scaling, which is the opposite trend than what was seen in figure 8 for the flame and the immediate post flame regions. This difference can be attributed to the different volumes and different residence times accordingly. The larger volume/longer residence time of the inner recirculation zone for constant velocity scaling is, however, compensated by a significant decrease of the mean volumetric rate compared to constant residence time scaling.

Figure 10 compares the NO_x formation rate at the 10 kW and the 100 kW scale based on the constant velocity scaling approach, as this represents a most severe increase in global NO_x. The contours are scaled to the same bluff body diameter, D. The inner recirculation zone can be recognized by the iso-lines corresponding to zero axial velocity. The normalized dimensions of the inner recirculation zone are comparable in both cases. In general, all conducted simulations predict a recirculation zone length of approximately 1.7 D. It can be seen that, at the laboratory scale of 10 kW, mainly the upper part of the inner recirculation zone contributes to the NO_x formation. The formation rate is in this region significantly lower at 100 kW. The contour plot shows furthermore a decrease of the formation rate in the flame and immediate post flame region, similar to what has been seen in figure 9. However, the local volumetric NO_x formation rate close to the flame anchor point is larger for 100 kW compared to 10 kW.

Thermal NO_x is the dominating NO_x route for the combustion of pure hydrogen at low pressures

This is the accepted version of an article published in Combustion and Flame
http://dx.doi.org/10.1016/j.combustflame.2020.01.010

and the temperature distribution is, therefore, an important factor for the overall NO_x formation rate. Figure 11 shows the mean temperature in the three dominating regions. The mean temperature in the inner recirculation zone is relatively constant and decreasing slightly at larger scales, for both scaling methodologies. Hence, the temperature cannot be the leading cause of the different trend for constant velocity and constant residence time scaling seen in figure 9. The spacial temperature distribution within the recirculation zone is, furthermore, relatively constant while the NO_x formation rate varies as has been seen in figure 10. The mean temperatures in the flame and immediate post flame region change slightly more with an approximately 8% decrease in the flame region and an similar large increase in the immediate post flame, when scaling with constant residence time from 10 kW to 500 kW. The mean temperature stays, on the other hand, nearly constant when constant velocity scaling is employed.

Since the temperatures in the flame and inner recirculation zone are generally sufficiently high for the formation of thermal NO_x, local species concentrations become the governing factor affecting NO_x formation. Thermal NO_x formation is described by the extended Zeldovich mechanism [52]. Hence, the driving radicals are O and OH, where the latter is important particularly at near stoichiometric conditions and fuel rich mixtures. Figure 12 shows the OH mass fraction distribution for the laboratory scale burner compared to the burner scaled to 100 kW following the two investigated scaling methodologies. The iso-lines show zero axial velocity to indicate the extend of the inner recirculation zone. It can be seen that the OH contours display a similar distribution as seen in figure 10 for the volumetric NO_x formation rate, with constant velocity scaling leading to lower and constant residence time scaling leading to higher OH mass fractions in the inner recirculation zone compared to the base case. A similar distribution in all three simulations was found for the O mass fraction, which is not shown here. The production of OH and O radicals is almost entirely attributed to the flame-sheet. Note that this is not referring to the flame region defined for post processing. Hence, the concentration of these two radicals in the inner recirculation zone is dependent on the flow conditions and the entrainment into inner recirculation zone. The entrainment is strongly affected

This is the accepted version of an article published in Combustion and Flame
http://dx.doi.org/10.1016/j.combustflame.2020.01.010

by the ratio between the penetration depth of the secondary fuel stream and the annular wall jet height, which is differently affected by the two applied scaling laws.

3.3. Constant velocity scaling up to 500 kW

The main flow features of the PPBB burner, namely an inner recirculation zone and a larger outer recirculation, where preserved in all simulations presented in the previous sections. The dimensions of these zones were, furthermore, relatively constant with a length of approximately 1.7 bluff body diameters for the inner and approximately 11 bluff body diameters for the outer recirculation zone. However, scaling the burner up to a scale of 500 kW based on constant velocity led to a fundamentally different flow field, causing the flame to impinge onto the combustion chamber wall, as can be seen in figure 13. The temperature contours, overlaid by the velocity vector field for the 10 kW and the 500 kW constant velocity simulations are compared in this figure. Sudden changes in the overall flame pattern, during scaling, have also been observed experimentally for other burners [35]. Applying constant residence time scaling on the other hand allowed to scale the burner successfully up to 500 kW, although, with the disadvantage of reaching high velocities. The simulation of the 250 kW and 500 kW scale with constant residence time scaling reached a local Mach number of 0.35 and 0.44 respectively, which exceed the upper limit of 0.3 generally applied as best practice for incompressible solvers. Both cases are still considered as subsonic flows, however, the model uncertainties introduced by neglecting compressibility effects become larger with increasing velocities.

Figure 13 shows the breakup of the inner recirculation zone at the 500 kW scale. Instead of the inner recirculation zone a set of two equally sized vortices is formed in the outer chamber region, which was previously characterized by a single large recirculation zone and smaller secondary vortices in regions of flow separation from the chamber wall. Note that only one of these secondary vortices is visible due to the coarsened resolution in the vector plot. These vortices cause the flame to be bend outwards leading to an impingement of high temperature flow onto the chamber wall. The breakup of the inner recirculation zone at this scale was only observed under reacting conditions.

This is the accepted version of an article published in Combustion and Flame
http://dx.doi.org/10.1016/j.combustflame.2020.01.010

An additional non-reacting simulation was conducted in which the original flow field, similar to the smaller scales, was preserved.

Based on the employed steady state RANS simulations it is not possible to determine if the breakup under reacting conditions is a transient flow instability or if the flow will remain permanently attach to the chamber wall. This could possibly be assessed by conducting unsteady RANS or scale resolving simulations. However, the more profound question is what causes the breakup of the inner recirculation zone. An apparent difference between the investigated scaling principles is the fuel concentration in the recirculation zone, which is an important factor for the flame stability [53]. Constant velocity scaling leads to an increased recirculation zone equivalence ratio, reaching 1.13 at the 450 kW scale, while constant residence time scaling leads to a decrease, reaching a lean equivalence ratio of 0.9 at the 500 kW scale. However, this effect is expected to be of less importance, since neither of the scaling laws leads to equivalence ratios far from stoichiometry.

Other important factors for the recirculation zone characteristics are the blockage ratio [53], the bluff body position [54], and the ratio between bluff body diameter and chamber diameter [35], which is 3.75 in the present study. However, these factors are not affected by the employed scaling methodologies. Hence, the breakup of the inner recirculation zone is most likely associated with a fundamental difference between the applied scaling methodologies. An inherent difference of the investigated scaling laws is the ratio between velocity and length scales, U_0/D_0, which is per definition constant for constant residence time scaling and decreases for constant velocity scaling. Hence, the annular jet flow for constant velocity scaling has a lower momentum compared to the flow for constant residence time scaling. The recirculation zone needs, furthermore, to span a significant larger distance when constant velocity scaling is applied as the bluff body diameter is larger compared to constant residence time scaling. This may indicate that the bluff body diameter and the annular throat cross section require independent scaling similar to what has been suggested by Cheng et al. [37].

It is not yet known if the breakup of the inner recirculation zone would also occur in an unconfined burner configuration. Hence, adjusting the chamber to bluff body diameter ratio may lead to

This is the accepted version of an article published in Combustion and Flame
http://dx.doi.org/10.1016/j.combustflame.2020.01.010

improved stability. Furthermore, the effect of different lance heights (i.e., the elevation of the bluff body with respect to the burner throat) on the recirculation zone could be explored. Tong et al. [54] suggested that the flame stability can be improved by modifying the bluff body position. However, altering the position of the conical bluff body changes inevitable also the cross-sectional throat area. This changes consequently the velocity of the annular jet flow, which will impact the flame stability as well and needs therefore to be investigated further.

4. Conclusion

Eleven CFD simulations of a complex burner configuration, at various scales ranging from 10 kW to 500 kW, were conducted. The characteristic combustion regimes and the NO_x emissions at the different scales were analysed, employing a novel approach of combining hexagonal binning and combustion regime diagrams. The scaling of the burner was conducted following two different scaling principles; the constant velocity and the constant residence time scaling.

Employing constant velocity scaling shifts the flame towards lower Karlovitz numbers and leads to combustion that spans multiple combustion regimes. The variation in the combustion regimes was shown to be less dependent on the local equivalence ratio compared to flames that were scaled by constant residence time scaling. Constant residence time scaling leads, on the other hand, to a constant global Damköhler number. However, a detailed analysis by means of CFD based regime diagrams showed that a considerable part of the flame follows a constant Karlovitz number, which is unexpected in relation to the theory of constant residence time scaling and evidenced the need for individual scaling laws for different burner regions.

Increasing the burner scale led, independent of the applied scaling law, to an increase of the total NO_x emissions. The fact that no plateau was reached within the investigated range and the observed Karlovitz number dependencies for constant residence time scaling suggest that the critical thermal load for the investigated burner was not reached. The immediate post flame, flame and inner recirculation zone regions dominate the NO_x formation while the influence of the post flame

This is the accepted version of an article published in Combustion and Flame
http://dx.doi.org/10.1016/j.combustflame.2020.01.010

and outer recirculation zone regions are negligible, which may explain the failure of global furnace residence time models to predict NO_x emissions at different burner scales.

Constant velocity scaling led to a lower total NO_x formation rate in the inner recirculation zone compared to constant residence time scaling, despite its larger volume and longer residence times. This was linked to the different effect that the scaling approaches have on the flow conditions and entrainment into the inner recirculation zone, such as the ratio between the penetration depth of the secondary fuel stream and the annular wall jet height. The entrainment affects consequently the O and OH concentrations, the dominating parameter for the NO_x formation in the inner recirculation zone.

A fundamental change of the flow field was observed in the narrow band between 450 kW and 500 kW scale when constant velocity scaling was applied. At this scale the inner recirculation zone breaks up and a vortex pair is formed in the outer region of the combustion chamber that causes the flame to be bend outwards and consequently impinge onto the chamber wall. Constant residence time scaling, on the other hand, preserved the inner recirculation zone at all investigated scales. The sudden breakup was attributed to the different effect of the scaling laws on the velocity to length scale ratio and momentum of the annular jet flow, and needs to be investigated further.

Acknowledgement

This publication has been produced with support from the BIGCCS Centre, performed under the Norwegian research program Centres for Environment-friendly Energy Research (FME). The authors acknowledge the following partners for their contributions: Gassco, Shell, Statoil, TOTAL, ENGIE and the Research Council of Norway (193816/S60). The CFD simulations were performed on resources provided by UNINETT Sigma2 - the National Infrastructure for High Performance Computing and Data Storage in Norway.

This is the accepted version of an article published in Combustion and Flame
http://dx.doi.org/10.1016/j.combustflame.2020.01.010

Appendix A Scaling

In what follows is the examination of the effect of constant velocity and constant residence time scaling on macro- and micro-mixing in terms of Damköhler and Karlovitz number, following the considerations made by Farcy et al. [55]. Given geometric similarity, all burner length scales, l, are increased by a factor, $\beta > 1$, when the burner is scaled up from laboratory scale to larger thermal loads:

$$l^* = \beta l, \tag{4}$$

where the star superscript represents scaled properties. For the following considerations it is furthermore assumed that the turbulent intensity stays unchanged for both scaling approaches.

A.1 Constant velocity scaling

Based on equation 2 the scaling factor for constant velocity scaling is:

$$\beta_v = \left(\frac{Q_v^*}{Q}\right)^{1/2}. \tag{5}$$

Since the velocity scale is unchanged, $u_v^* = u$, and all length scales are scaled up, $l_v^* = \beta_v l$, we obtain:

$$k_v^{*1/2} \approx l_v'^* \left|\frac{\partial u_v^*}{\partial y_v^*}\right| = \beta_v l' \left|\frac{1}{\beta_v}\frac{\partial u}{\partial y}\right| = k^{1/2}, \tag{6}$$

where k is the turbulent kinetic energy. Furthermore we see that the turbulent Reynolds number, Re_T, scales with the factor β_v:

$$Re_{T,v}^* = \frac{k_v^{*1/2} l_v'^*}{\nu} = \frac{k^{1/2}\beta_v l'}{\nu} = \beta_v Re_T, \tag{7}$$

the Kolmogorov scale, η_k, scales with the factor $\beta_v^{1/4}$:

$$\eta_{k,v}^* \approx \frac{l_v'^*}{{Re_{T,v}^*}^{3/4}} = \frac{\beta_v l'}{(\beta_v Re_T)^{3/4}} = \beta_{rt}^{1/4}\eta_k, \tag{8}$$

and the dissipation rate, ϵ, scales with the factor β_v^{-1}:

$$\epsilon_v^* \approx \frac{\nu^3}{{\eta_{k,v}^*}^4} = \frac{\nu^3}{\left(\beta_v^{1/4}\eta_k\right)^4} = \frac{1}{\beta_v}\epsilon. \tag{9}$$

This is the accepted version of an article published in Combustion and Flame
http://dx.doi.org/10.1016/j.combustflame.2020.01.010

As a result, the turbulent time scale, τ_T, scales with the factor β_v:

$$\tau^*_{T,v} = \frac{k^*_v}{\epsilon^*_v} = \frac{k}{\beta_v^{-1}\epsilon} = \beta_v \tau_T, \tag{10}$$

and the Kolmogorov time scale, τ_k, with the factor $\beta_v^{1/2}$:

$$\tau^*_{k,v} = \left(\frac{\nu}{\epsilon^*_v}\right)^{1/2} = \left(\frac{\nu}{\beta_v^{-1}\epsilon}\right)^{1/2} = \beta_v^{1/2}\tau_k. \tag{11}$$

The scaling relation for the Damköhler number is thus:

$$Da^*_v = \frac{\tau^*_{T,v}}{\tau^*_{c,v}} = \frac{\beta_v \tau_T}{\tau_c} = \beta_v Da, \tag{12}$$

and for the Karlovitz number:

$$Ka^*_v = \frac{\tau^*_{c,v}}{\tau^*_{k,v}} = \frac{\tau_c}{\beta_v^{1/2}\tau_k} = \frac{1}{\beta_v^{1/2}} Ka. \tag{13}$$

Substituting β_v with equation (5) leads to:

$$Da^*_v = \left(\frac{Q^*_v}{Q}\right)^{1/2} Da, \tag{14}$$

and

$$Ka^*_v = \left(\frac{Q^*_v}{Q}\right)^{-1/4} Ka. \tag{15}$$

A.2 Constant residence time scaling

Based on equation 3 the scaling factor for constant residence time scaling is:

$$\beta_{rt} = \left(\frac{Q^*_{rt}}{Q}\right)^{1/3}. \tag{16}$$

Additionally to the length scales also the velocity needs to be scaled up, $u^*_{rt} = \beta_{rt} u$, in order to preserve the residence time, which leads to:

$$k^{*\,1/2}_{rt} \approx l'^{\,*}_{rt} \left|\frac{\partial u^*_{rt}}{\partial y^*_{rt}}\right| = \beta_{rt} l' \left|\frac{\beta_{rt}}{\beta_{rt}}\frac{\partial u}{\partial y}\right| = \beta_{rt} k^{1/2}, \tag{17}$$

This is the accepted version of an article published in Combustion and Flame
http://dx.doi.org/10.1016/j.combustflame.2020.01.010

505 or equivalently

$$k^*_{rt} = \beta^2_{rt} k. \tag{18}$$

506 Here the turbulent Reynolds number, Re_T, scales with the factor β^2_{rt}:

$$Re^*_{T,rt} = \frac{{k^*_{rt}}^{1/2} {l'_{rt}}^*}{\nu} = \frac{\beta_{rt} k^{1/2} \beta_{rt} l'}{\nu} = \beta^2_{rt} Re_T, \tag{19}$$

507 the Kolmogorov scale, η_k, scales with the factor $\beta^{-1/2}_{rt}$:

$$\eta^*_{k,rt} \approx \frac{{l'_{rt}}^*}{{Re^*_{T,rt}}^{3/4}} = \frac{\beta_{rt} l'}{(\beta^2_{rt} Re_T)^{3/4}} = \frac{1}{\beta^{1/2}_{rt}} \eta_k, \tag{20}$$

508 and the dissipation rate, ϵ, scales with the factor β^2_{rt}:

$$\epsilon^*_{rt} \approx \frac{\nu^3}{{\eta^*_{k,rt}}^4} = \frac{\nu^3}{\left(\beta^{-1/2}_{rt} \eta_k\right)^4} = \beta^2_{rt} \epsilon. \tag{21}$$

509 This leads to a constant turbulent time scale, τ_T:

$$\tau^*_{T,rt} = \frac{k^*_{rt}}{\epsilon^*_{rt}} = \frac{\beta^2_{rt}}{\beta^2_{rt}} \frac{k}{\epsilon} = \tau_T, \tag{22}$$

510 and a scaled Kolmogorov time, τ_k, by the factor β^{-1}_{rt}:

$$\tau^*_{k,rt} = \left(\frac{\nu}{\epsilon^*_{rt}}\right)^{1/2} = \left(\frac{\nu}{\beta^2_{rt} \epsilon}\right)^{1/2} = \frac{1}{\beta_{rt}} \tau_k. \tag{23}$$

511 The Damköhler number, Da, representing macro-mixing is thus constant for a fixed chemical time
512 scale, $\tau^*_{c,rt} = \tau_c$:

$$Da^*_{rt} = \frac{\tau^*_{T,rt}}{\tau^*_{c,rt}} = \frac{\tau_T}{\tau_c} = Da. \tag{24}$$

513 The Karlovitz number, Ka, that represents micro-mixing on the other hand scales with factor β_{rt}:

$$Ka^*_{rt} = \frac{\tau^*_{c,rt}}{\tau^*_{k,rt}} = \frac{\tau_c}{\beta^{-1}_{rt} \tau_k} = \beta_{rt} Ka, \tag{25}$$

514 which together with equation (16) leads to:

$$Ka^*_{rt} = \left(\frac{Q^*_{rt}}{Q}\right)^{1/3} Ka. \tag{26}$$

This is the accepted version of an article published in Combustion and Flame
http://dx.doi.org/10.1016/j.combustflame.2020.01.010

Equation (14) and (15) together with equation (24) and (26) show the inherent problem of scaling turbulent flames, namely that the non-linear character of turbulence makes it impossible to preserve both macro- and micro-mixing, even when the majority of other non-dimensional groups are neglected. Hence, one needs to decide which mixing mechanism is given the higher priority by choosing an appropriate scaling law. The present work discusses the effect of this on the combustion characteristics of of complex low emission burners, here represented by the PPBB burner.

References

[1] H. Kobayashi, A. Hayakawa, K. Somarathne, E. Okafor, Science and technology of ammonia combustion, Proceedings of the Combustion Institute 37 (1) (2019) 109–133. doi:10.1016/j.proci.2018.09.029.

[2] D. Dunn-Rankin, P. Therkelsen (Eds.), Lean Combustion, 2nd Edition, Academic Press, 2016.

[3] A. Uemichi, K. Kouzaki, K. Warabi, K. Shimamura, M. Nishioka, Formation of ultra-lean comet-like flame in swirling hydrogen–air flow, Combustion and Flame 196 (2018) 314–324. doi:10.1016/j.combustflame.2018.06.019.

[4] P. Stuttaford, H. Rizkalla, Y. Chen, B. Copley, T. Faucett, Extended Turndown, Fuel Flexible Gas Turbine Combustion System, in: Volume 2: Combustion, Fuels and Emissions, Parts A and B, ASME, 2010, pp. 483–492. doi:10.1115/GT2010-22585.

[5] A. Haj Ayed, K. Kusterer, H.-W. Funke, J. Keinz, C. Striegan, D. Bohn, Improvement study for the dry-low-NOx hydrogen micromix combustion technology, Propulsion and Power Research 4 (3) (2015) 132–140. doi:10.1016/j.jppr.2015.07.003.

[6] M. Dutka, M. Ditaranto, T. Løvås, NOx emissions and turbulent flow field in a partially premixed bluff body burner with CH4 and H2 fuels, International Journal of Hydrogen Energy 41 (28) (2016) 12397–12410. doi:10.1016/j.ijhydene.2016.05.154.

This is the accepted version of an article published in Combustion and Flame
http://dx.doi.org/10.1016/j.combustflame.2020.01.010

[7] K. Souflas, P. Koutmos, On the non-reacting flow and mixing fields of an axisymmetric disk stabilizer, under inlet mixture stratification and preheat, Experimental Thermal and Fluid Science 99 (2018) 357–366. doi:10.1016/j.expthermflusci.2018.08.008.

[8] D. Spalding, The art of partial modeling, Symposium (International) on Combustion 9 (1) (1963) 833–843. doi:10.1016/S0082-0784(63)80090-9.

[9] J. Beér, The Significance of Modelling, Journal of Insitute of Fuel 39 (1966) 466–473.

[10] S. R. Turns, Understanding NOx formation in nonpremixed flames: experiments and modeling, Prog. Energy Combust. Sci. 21 (1995) 361–385.

[11] M. Sadakata, Y. Hirose, Scaling law for pollutant emission from a combustion furnace, Fuel 73 (8) (1994) 1338–1342. doi:10.1016/0016-2361(94)90310-7.

[12] R. Weber, Scaling characteristics of aerodynamics, heat transfer, and pollutant emissions in industrial flames, Symposium (International) on Combustion 26 (2) (1996) 3343–3354. doi:10.1016/S0082-0784(96)80182-2.

[13] G. A. Lavoie, A. F. Schlander, A Scaling Study of NO Formation in Turbulent Diffusion Flames of Hydrogen Burning in Air, Combustion Science and Technology 8 (5-6) (1973) 215–224. doi:10.1080/00102207308946645.

[14] N. Peters, An Asymptotic Analysis of Nitric Oxide Formation in Turbulent Diffusion Flames, Combustion Science and Technology 19 (1-2) (1978) 39–49. doi:10.1080/00102207808946862.

[15] M. C. Drake, R. J. Blint, Thermal NOx in stretched laminar opposed-flow diffusion flames with CO/H2/N2 fuel, Combustion and Flame 76 (2) (1989) 151–167. doi:10.1016/0010-2180(89)90064-3.

This is the accepted version of an article published in Combustion and Flame
http://dx.doi.org/10.1016/j.combustflame.2020.01.010

[16] R. Barlow, C. Carter, Raman/Rayleigh/LIF measurements of nitric oxide formation in turbulent hydrogen jet flames, Combustion and Flame 97 (3-4) (1994) 261–280. doi:10.1016/0010-2180(94)90020-5.

[17] C. D. Carter, R. S. Barlow, Simultaneous measurements of NO, OH, and the major species in turbulent flames, Optics Letters 19 (4) (1994) 299. doi:10.1364/OL.19.000299.

[18] J. Kent, R. Bilger, The prediction of turbulent diffusion flame fields and nitric oxide formation, Symposium (International) on Combustion 16 (1) (1977) 1643–1656. doi:10.1016/S0082-0784(77)80443-8.

[19] R.-H. Chen, J. F. Driscoll, Nitric oxide levels of jet diffusion flames: Effects of coaxial air and other mixing parameters, Symposium (International) on Combustion 23 (1) (1991) 281–288. doi:10.1016/S0082-0784(06)80271-7.

[20] J.-Y. Chen, W. Kollmann, PDF modeling and analysis of thermal NO formation in turbulent nonpremixed hydrogen-air jet flames, Combustion and Flame 88 (3-4) (1992) 397–412. doi:10.1016/0010-2180(92)90042-N.

[21] N. Smith, R. Bilger, J.-Y. Chen, Modelling of nonpremixed hydrogen jet flames using a conditional moment closure method, Symposium (International) on Combustion 24 (1) (1992) 263–269. doi:10.1016/S0082-0784(06)80035-4.

[22] G. Szego, B. Dally, G. Nathan, Scaling of NOx emissions from a laboratory-scale mild combustion furnace, Combustion and Flame 154 (1-2) (2008) 281–295. doi:10.1016/j.combustflame.2008.02.001.

[23] S. R. Turns, F. H. Myhr, Oxides of nitrogen emissions from turbulent jet flames: Part I—Fuel effects and flame radiation, Combustion and Flame 87 (3-4) (1991) 319–335. doi:10.1016/0010-2180(91)90116-S.

This is the accepted version of an article published in Combustion and Flame
http://dx.doi.org/10.1016/j.combustflame.2020.01.010

[24] S. R. Turns, F. H. Myhr, R. V. Bandaru, E. R. Maund, Oxides of nitrogen emissions from turbulent jet flames: Part II—Fuel dilution and partial premixing effects, Combustion and Flame 93 (3) (1993) 255–269. doi:10.1016/0010-2180(93)90107-E.

[25] A. Lutz, R. Kee, R. Dibble, J. Broadwell, A model for detailed chemical kinetics in turbulent nonpremixed jet flames, in: 29th Aerospace Sciences Meeting, American Institute of Aeronautics and Astronautics, Reston, Virigina, 1991. doi:10.2514/6.1991-478.

[26] N. A. Røkke, J. E. Hustad, O. K. Sønju, A study of partially premixed unconfined propane flames, Combustion and Flame 97 (1) (1994) 88–106. doi:10.1016/0010-2180(94)90118-X.

[27] A. Santos, M. Costa, Reexamination of the scaling laws for NOx emissions from hydrocarbon turbulent jet diffusion flames, Combustion and Flame 142 (1-2) (2005) 160–169. doi:10.1016/j.combustflame.2005.03.004.

[28] R. Weber, J. F. Driscoll, W. J. Dahm, R. T. Waibel, Scaling Characteristics of Aerodynamics and Low-NOx Properties of Industrial Natural Gas Burners. The SCALING 400 Study. Part I: Test Plan, Tech. rep., GRI Topoical Report 93/0227, Gas Research Institute, Chicago (1993).

[29] U. Bollettini, F. Breussin, R. Weber, A study on scaling of natural gas burners, IFRF Combustion Journal.

[30] R. Weber, F. Breussin, Scaling properties of swirling pulverized coal flames: From 180 kW to 50 MW thermal input, Symposium (International) on Combustion 27 (2) (1998) 2957–2964. doi:10.1016/S0082-0784(98)80155-0.

[31] J. P. Smart, W. L. D. Van Kamp, The Impact of Scaling Criteria on the Characteristics of Pulverised Coal Flames, Developments in Chemical Engineering and Mineral Processing 7 (3-4) (1999) 301–331. doi:10.1002/apj.5500070305.

This is the accepted version of an article published in Combustion and Flame
http://dx.doi.org/10.1016/j.combustflame.2020.01.010

[32] N. Megalos, N. Smith, D. Zhang, The potential for low NOx from a precessing jet burner of coal, Combustion and Flame 124 (1-2) (2001) 50–64. doi:10.1016/S0010-2180(00)00173-5.

[33] H. Levinsky, C. van der Meij, LIF and CARS measurements performed on the 50 kW bluff-body burner for the British Gas, Tech. rep., Gaz de France, Gasunie, GRI collaboration, N.V. Nederlandse Gasunie (1994).

[34] M. Perrin, J. Imbach, S. Albert, J. Mariasine, British Gas/Gasunie/Gaz de France collaboration on turbulent diffusion flames scaling. Velocity, Temperature and Concentration Measurements on a 500 kW Bluff-Body Burner, Tech. rep., Gas de France (1994).

[35] R. Weber, M. Mancini, On scaling and mathematical modelling of large scale industrial flames, Journal of the Energy Institutedoi:10.1016/j.joei.2019.04.010.

[36] T.-C. Hsieh, W. J. Dahm, J. F. Driscoll, Scaling Laws for NOx Emission Performance of Burners and Furnaces from 30 kW to 12 MW, Combustion and Flame 114 (1-2) (1998) 54–80. doi:10.1016/S0010-2180(97)00289-7.

[37] R. Cheng, D. Yegian, M. Miyasato, G. Samuelsen, C. Benson, R. Pellizzari, P. Loftus, Scaling and development of low-swirl burners for low-emission furnaces and boilers, Proceedings of the Combustion Institute 28 (1) (2000) 1305–1313. doi:10.1016/S0082-0784(00)80344-6.

[38] Ø. Spangelo, O. Sonju, T. Slungaard, M. Ditaranto, US 20090220899 A1 (2009).

[39] M. Dutka, Emissions of nitrogen oxides from partially premixed flames stabilized on a conical bluff body, Ph.D. thesis, NTNU (2015).

[40] M. Dutka, M. Ditaranto, T. Løvås, Application of a Central Composite Design for the Study of NOx Emission Performance of a Low NOx Burner, Energies 8 (5) (2015) 3606–3627. doi:10.3390/en8053606.

This is the accepted version of an article published in Combustion and Flame
http://dx.doi.org/10.1016/j.combustflame.2020.01.010

[41] M. Dutka, M. Ditaranto, T. Løvås, Emission characteristics of a novel low NO x burner fueled by hydrogen-rich mixtures with methane, Journal of Power Technologies 95 (2) (2015) 105–111.

[42] C. Meraner, T. Li, M. Ditaranto, T. Løvås, Cold flow characteristics of a novel bluff body hydrogen burner, International Journal of Hydrogen Energy 43 (14) (2018) 7155–7168. doi:10.1016/j.ijhydene.2018.02.062.

[43] C. Meraner, T. Li, M. Ditaranto, T. Løvås, Combustion and NO x Emission Characteristics of a Bluff Body Hydrogen Burner, Energy & Fuels 33 (5) (2019) 4598–4610. doi:10.1021/acs.energyfuels.9b00313.

[44] B. Magnussen, On the structure of turbulence and a generalized eddy dissipation concept for chemical reaction in turbulent flow, in: 19th Aerospace Sciences Meeting, American Institute of Aeronautics and Astronautics, Reston, Virigina, 1981, pp. 1–6. doi:10.2514/6.1981-42.

[45] B. Magnussen, B. Hjertager, On mathematical modeling of turbulent combustion with special emphasis on soot formation and combustion, Symposium (International) on Combustion 16 (1) (1977) 719–729. doi:10.1016/S0082-0784(77)80366-4.

[46] J. Li, Z. Zhao, A. Kazakov, F. L. Dryer, An updated comprehensive kinetic model of hydrogen combustion, International Journal of Chemical Kinetics 36 (10) (2004) 566–575. doi:10.1002/kin.20026.

[47] J. R. Nanduri, D. R. Parsons, S. L. Yilmaz, I. B. Celik, P. A. Strakey, Assessment of RANS-Based Turbulent Combustion Models for Prediction of Emissions from Lean Premixed Combustion of Methane, Combustion Science and Technology 182 (7) (2010) 794–821. doi:10.1080/00102200903341546.

[48] D. A. Lysenko, I. S. Ertesvåg, Reynolds-Averaged, Scale-Adaptive and Large-Eddy Simulations

This is the accepted version of an article published in Combustion and Flame
http://dx.doi.org/10.1016/j.combustflame.2020.01.010

of Premixed Bluff-Body Combustion Using the Eddy Dissipation Concept, Flow, Turbulence and Combustion 100 (3) (2018) 721–768. doi:10.1007/s10494-017-9880-4.

[49] N. Lewin-Koh, Hexagon Binning: an Overview, Tech. rep., TU Dortmund (2009).

[50] N. Peters, The turbulent burning velocity for large-scale and small-scale turbulence, Journal of Fluid Mechanics 384 (1999) S0022112098004212. doi:10.1017/S0022112098004212.

[51] D. G. Goodwin, R. L. Speth, H. K. Moffat, B. W. Weber, Cantera: An object-oriented software toolkit for chemical kinetics, thermodynamics, and transport processes (2018). doi:10.5281/zenodo.1174508.

[52] Y. B. Zeldovich, The oxidation of nitrogen in combustion and explosions, Acta Physicochimica U.R.S.S. 21 (1946) 577–628.

[53] R. W. Schefer, M. Namazian, J. Kelly, M. Perrin, Effect of Confinement on Bluff-Body Burner Recirculation Zone Characteristics and Flame Stability, Combustion Science and Technology 120 (1-6) (1996) 185–211. doi:10.1080/00102209608935573.

[54] Y. Tong, M. Li, J. Klingmann, S. Chen, Z. Li, Experimental Investigation on the Influences of Bluff-Body's Position on Diffusion Flame Structures, in: Volume 1: Boilers and Heat Recovery Steam Generator; Combustion Turbines; Energy Water Sustainability; Fuels, Combustion and Material Handling; Heat Exchangers, Condensers, Cooling Systems, and Balance-of-Plant, ASME, 2017, p. V001T04A009. doi:10.1115/POWER-ICOPE2017-3090.

[55] B. Farcy, L. Vervisch, P. Domingo, Large eddy simulation of selective non-catalytic reduction (SNCR): A downsizing procedure for simulating nitric-oxide reduction units, Chemical Engineering Science 139 (2015) 285–303. doi:10.1016/j.ces.2015.10.002.

This is the accepted version of an article published in Combustion and Flame
http://dx.doi.org/10.1016/j.combustflame.2020.01.010

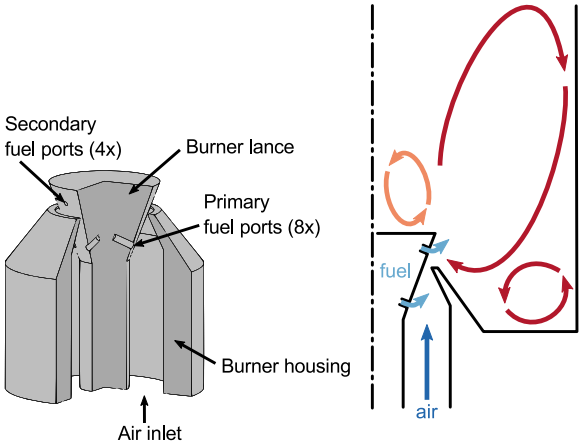

Figure 1: 3D rendering of the PPBB burner and illustration of the flow pattern. Primary and secondary fuel ports are drawn in the same plane for illustration purpose.

This is the accepted version of an article published in Combustion and Flame
http://dx.doi.org/10.1016/j.combustflame.2020.01.010

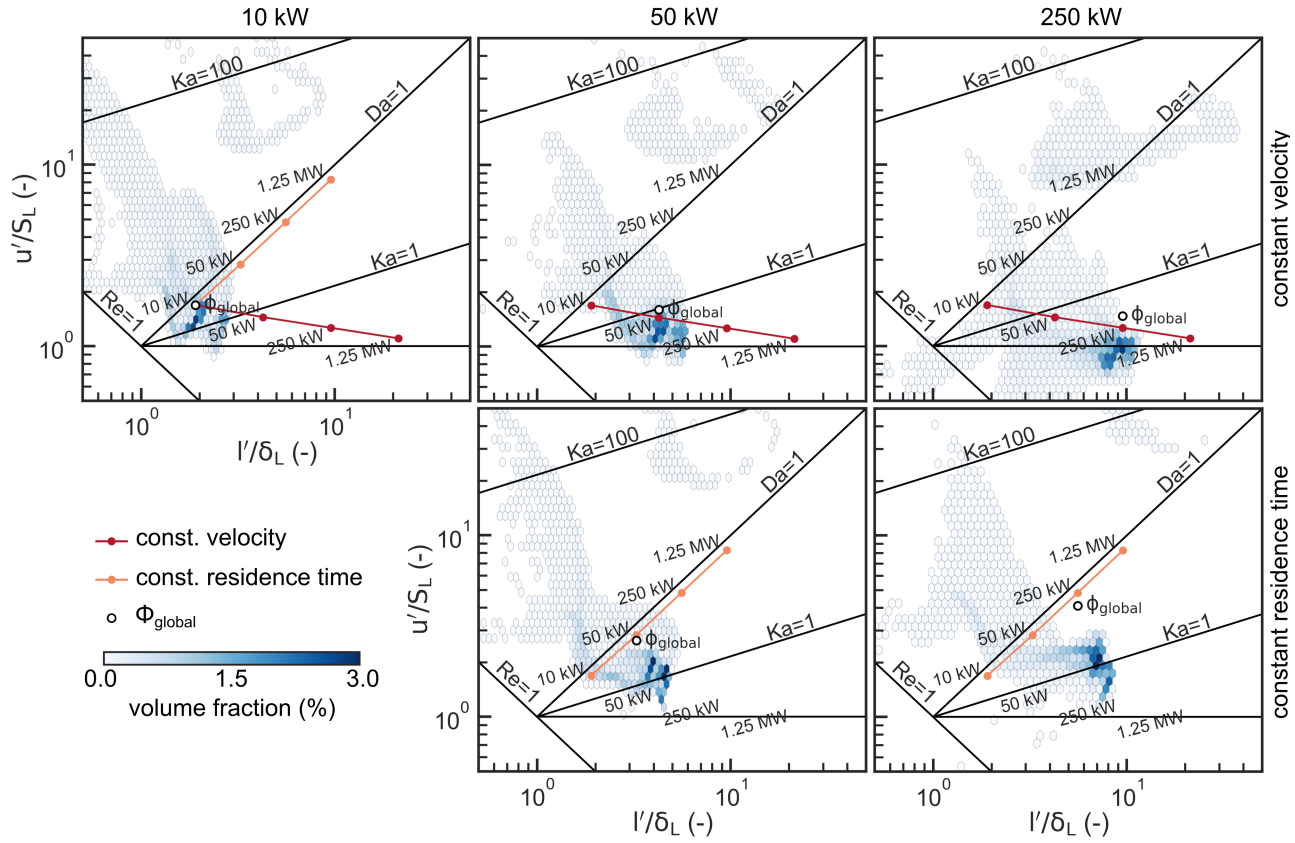

Figure 2: Modified turbulent combustion diagram based on Peters [50]. The hexbin distribution is obtained from CFD simulations and coloured by the volume fraction that is represented by each bin (i.e., the volume associated to one single bin normalized by the total volume represented in the hexbin plot). The red and orange lines show the theoretical scaling for the global burner representation. The single circular marker shows the global representation of the burner within the regime diagram.

This is the accepted version of an article published in Combustion and Flame
http://dx.doi.org/10.1016/j.combustflame.2020.01.010

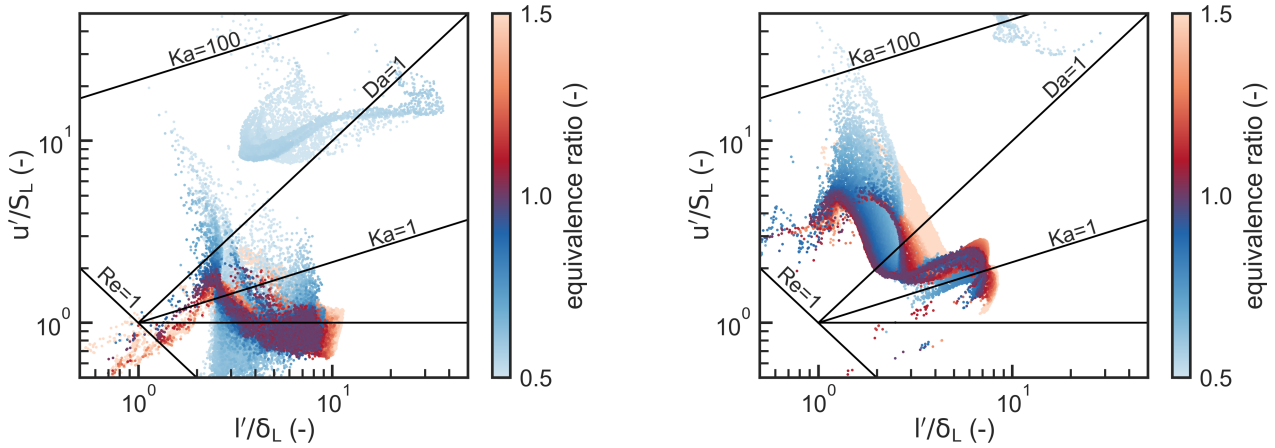

(a) constant velocity scaling

(b) constant residence time scaling

Figure 3: Modified turbulent combustion diagram based on Peters [50] containing the scatter plot for the burner at the 250 kW scale based in the two different scaling laws. The scatter plot is coloured by the local equivalence ratio. Data points closed to stoichiometric conditions overlap data points that are further away.

This is the accepted version of an article published in Combustion and Flame
http://dx.doi.org/10.1016/j.combustflame.2020.01.010

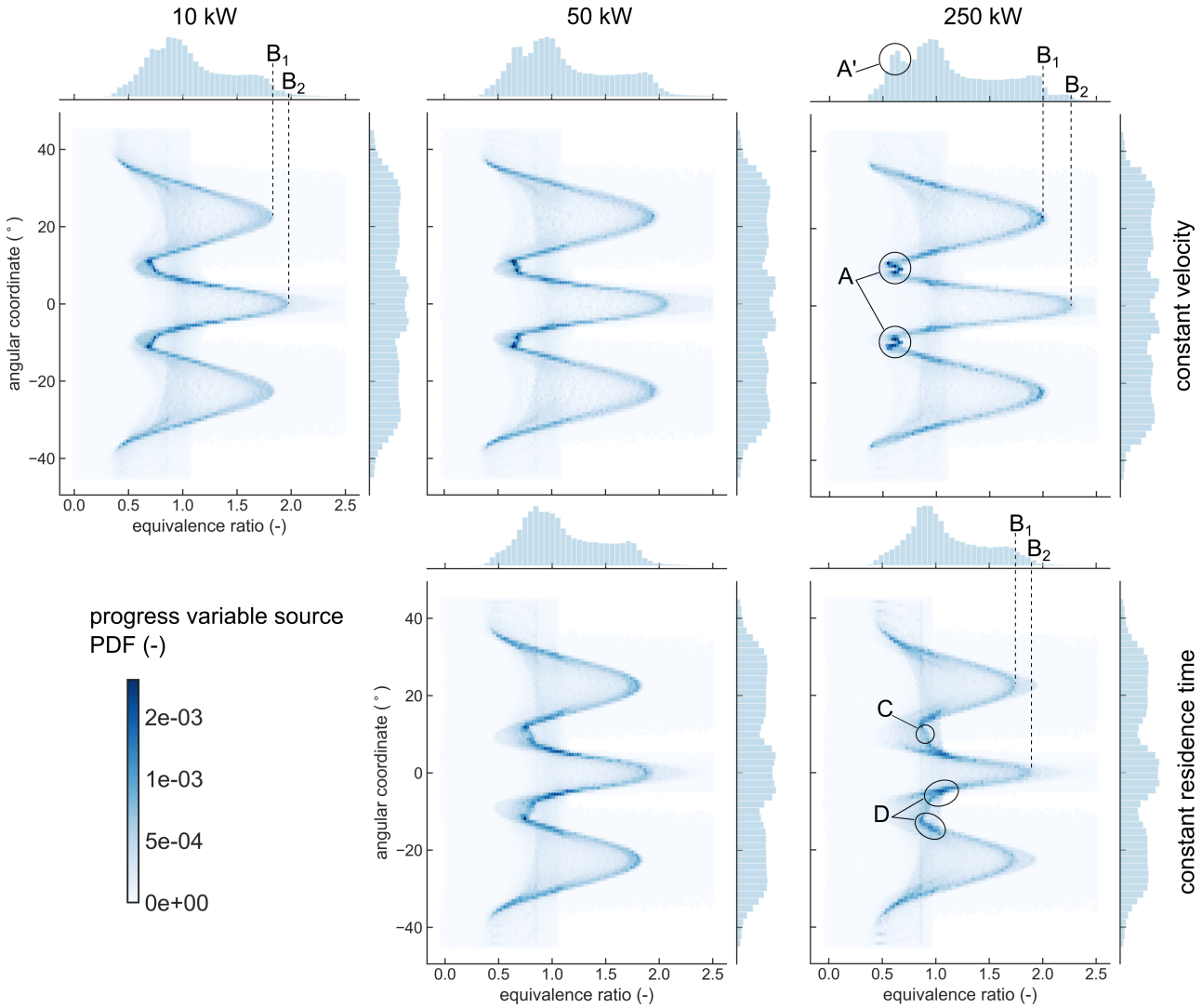

Figure 4: Hexbin plot of the the progress variable source term probability density distribution integrated along axial and radial direction, plotted in a two dimensional space formed by the equivalence ratio and the angular coordinate. The marginal plots show the probability density function of the progress variable source term along the corresponding axes.

This is the accepted version of an article published in Combustion and Flame
http://dx.doi.org/10.1016/j.combustflame.2020.01.010

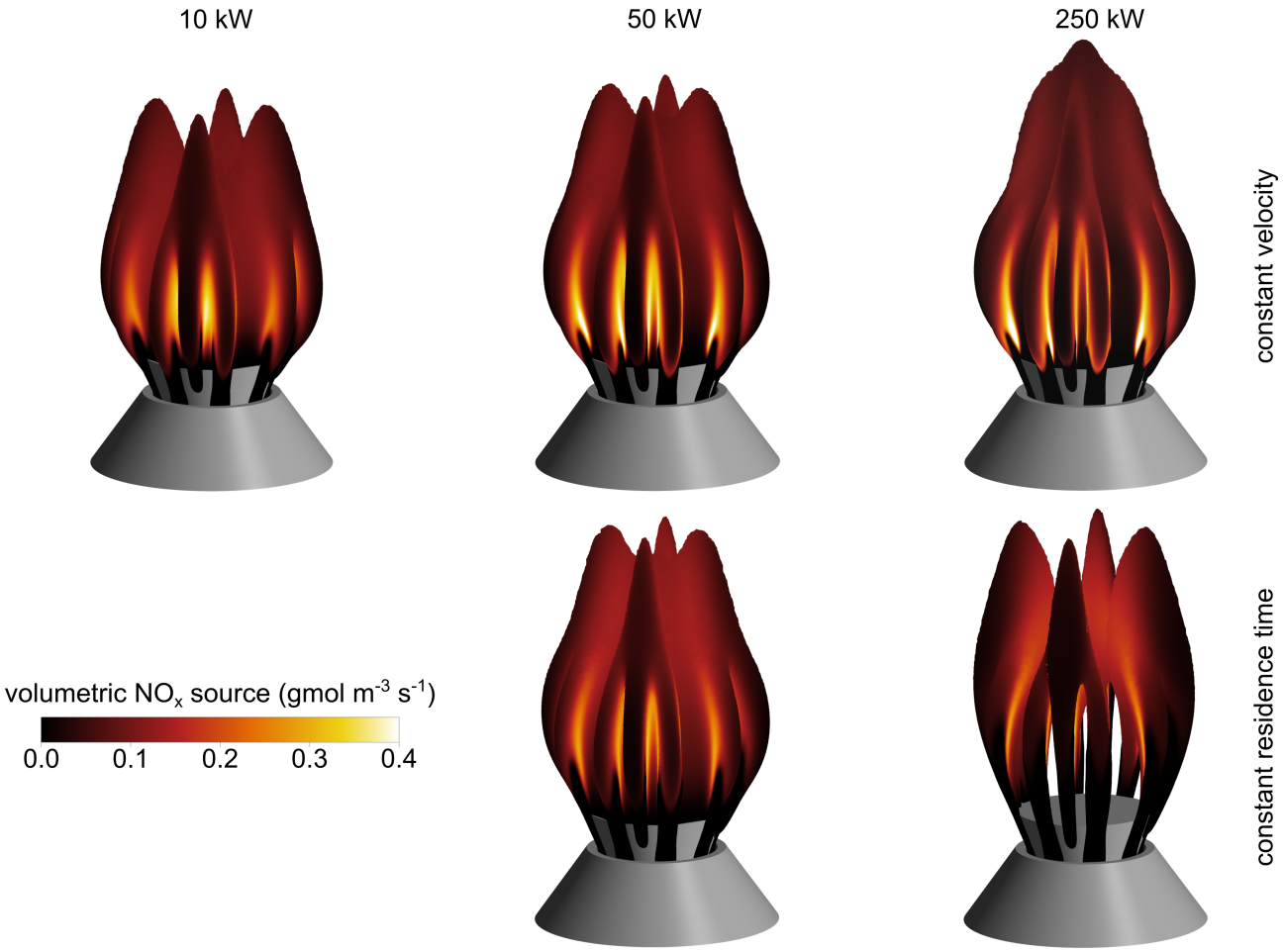

Figure 5: Iso-surface of the stoichiometric equivalence ratio coloured by the NO_x formation rate.

This is the accepted version of an article published in Combustion and Flame
http://dx.doi.org/10.1016/j.combustflame.2020.01.010

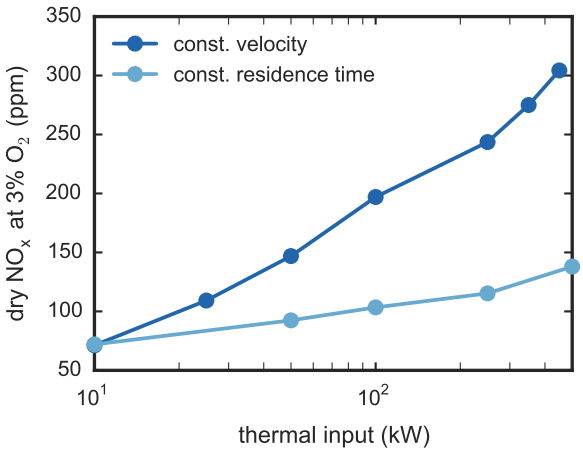

Figure 6: Global NO_x emissions monitored at the chamber outlet.

This is the accepted version of an article published in Combustion and Flame
http://dx.doi.org/10.1016/j.combustflame.2020.01.010

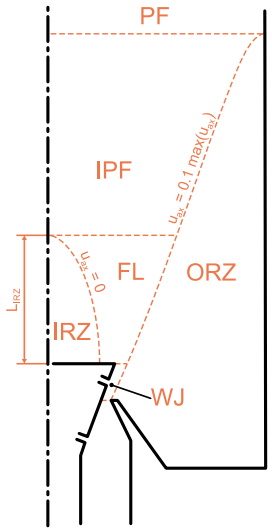

Figure 7: Illustration of the post processing regions. Note the zones are not to scale and the fuel ports are drawn in the same plane for illustration purpose.

This is the accepted version of an article published in Combustion and Flame
http://dx.doi.org/10.1016/j.combustflame.2020.01.010

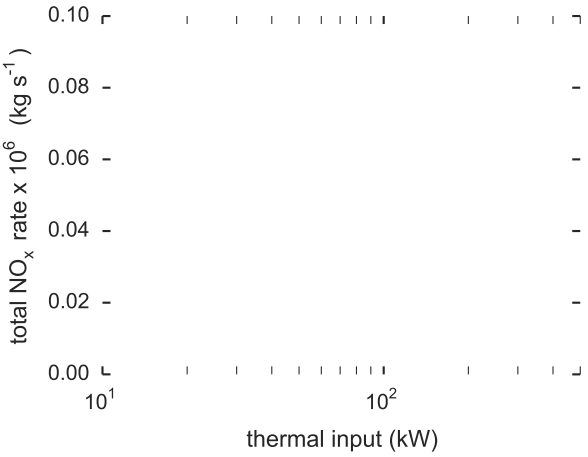

Figure 8: Volume integral of the volumetric NO_x formation rate. Solid lines and filled marker show constant velocity scaling, while dashed lines and open marker show constant residence time scaling.

This is the accepted version of an article published in Combustion and Flame
http://dx.doi.org/10.1016/j.combustflame.2020.01.010

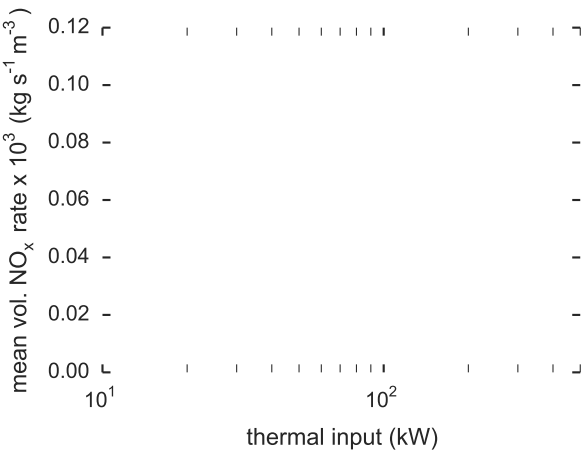

Figure 9: Volume weighted average volumetric NO_x formation rate. Solid lines and filled marker show constant velocity scaling, while dashed lines and open marker show constant residence time scaling.

This is the accepted version of an article published in Combustion and Flame
http://dx.doi.org/10.1016/j.combustflame.2020.01.010

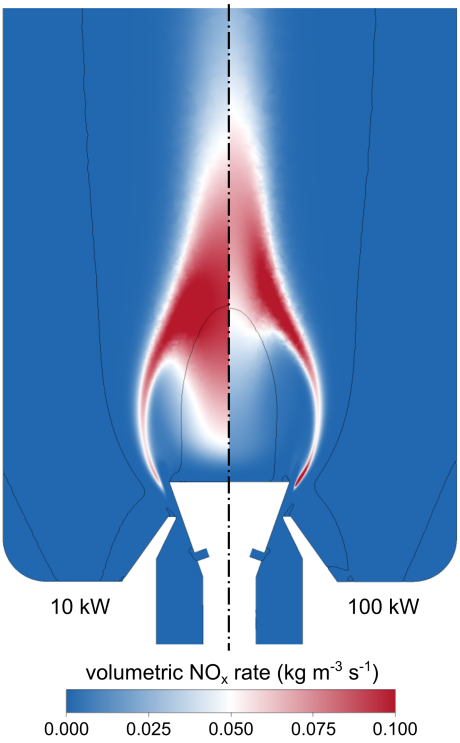

Figure 10: Volumetric NO_x formation rate contours for 10 kW (left) and 100 kW (right) thermal input, where the latter was scaled based on constant velocity scaling. The black iso-lines indicate a zero axial velocity component. Note that the dimensions in the figure are normalized by the bluff body diameter.

This is the accepted version of an article published in Combustion and Flame
http://dx.doi.org/10.1016/j.combustflame.2020.01.010

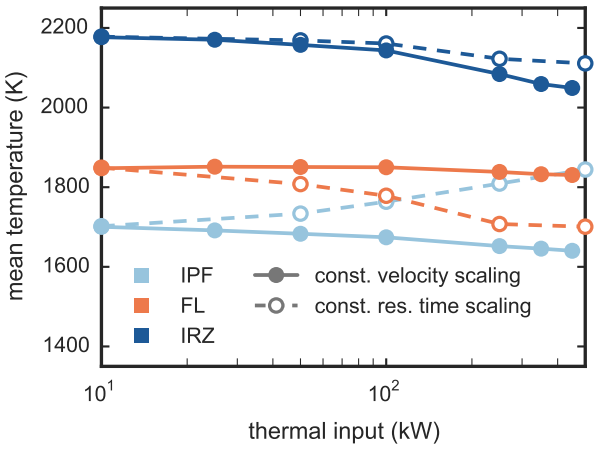

Figure 11: Volume weighted average temperature. Solid lines and filled marker show constant velocity scaling, while dashed lines and open marker show constant residence time scaling.

This is the accepted version of an article published in Combustion and Flame
http://dx.doi.org/10.1016/j.combustflame.2020.01.010

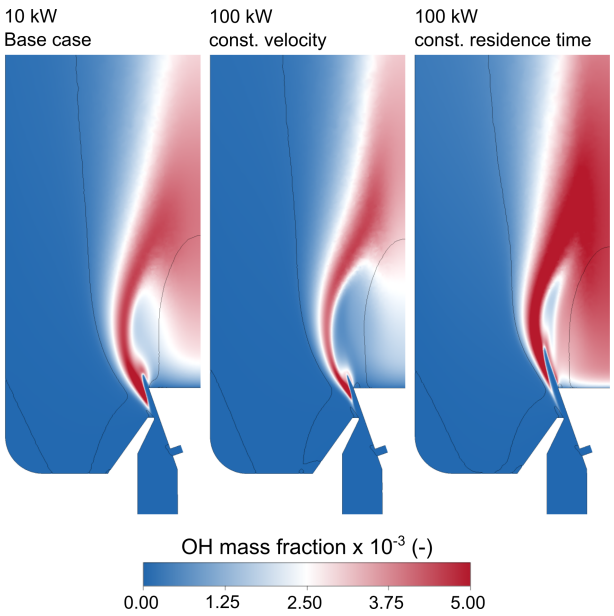

Figure 12: Contours of the OH mass fraction distribution. The black iso-lines indicate a zero axial velocity component. The size of all figures is normalized by the bluff body diameter.

This is the accepted version of an article published in Combustion and Flame
http://dx.doi.org/10.1016/j.combustflame.2020.01.010

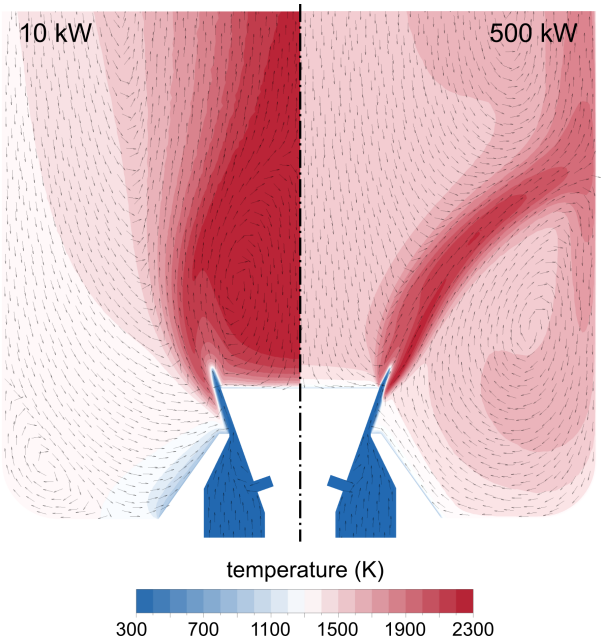

Figure 13: Temperature contours overlaid by the velocity vector field for 10 kW (left) and 500 kW (right) thermal input, where the latter was scaled based on constant velocity scaling. The size of both contours is normalized by the bluff body diameter.

This is the accepted version of an article published in Combustion and Flame
http://dx.doi.org/10.1016/j.combustflame.2020.01.010